

# Ca mobility in NASICON battery materials studied from first principles

Katharina Helmbrecht<sup>\*,†</sup> and Axel Groß<sup>†,‡</sup>

<sup>†</sup>*Institute of Theoretical Chemistry, Ulm University, Mez-Starck-Haus Oberberghof 7, 89081  
Ulm, Germany*

<sup>‡</sup>*Helmholtz Institute Ulm (HIU) for Electrochemical Energy Storage, Helmholtzstraße 11,  
89081 Ulm, Germany*

E-mail: [katharina.helmbrecht@uni-ulm.de](mailto:katharina.helmbrecht@uni-ulm.de)

## Abstract

Batteries using multivalent charge carriers present a promising alternative to traditional Li-ion technology, offering the potential for higher energy densities and often relying on more abundant elements. However, their ion mobility within the electrolyte and cathode is generally lower than that of monovalent carriers due to stronger electrostatic interactions, heightening the need for materials that can provide high ion mobility. NASICON materials are known for their high ion mobility with monovalent carriers and are widely used as solid electrolytes. In this computational study, we investigate calcium ion mobility in two NASICON materials, focusing on how the transition metal's atomic size influences the height of the migration barrier and the properties of the materials as a solid electrolyte or electrode material.

## Introduction

Today, most of the demand for portable energy storage is met by lithium-ion batteries (LIBs), which is largely due to their extraordinary performance, including high energy density, operating voltage and long life cycle.<sup>1,2</sup> However, problems arise in sourcing the needed lithium and cobalt metal,<sup>3</sup> meaning that state of the art LIBs may not be able to fulfill the growing demand for energy storage solutions. Hence, alternative battery concepts and new battery materials are needed which allow for sustainable, safe, compact and high voltage energy storage systems.<sup>4-7</sup> While it seems unlikely that alternative battery technologies will be able to surpass Li in the area of portable batteries, there is also a growing demand for stationary energy storage and heavy-duty systems. The requirements of those can, on the other hand, be met by a variety of battery types.

NASICON sodium (Na) super ionic conductor structures exhibit great structural stability and high ionic conductivity - especially for sodium ions.<sup>8</sup> They belong to the family of superionic conductors, which are materials that display exceptionally high ionic conductivity at or near room temperature.<sup>9</sup> Furthermore, they are classified as a polyanionic compounds,

meaning they contain anions with multiple negative charges, such as the characteristic, tetrahedral anionic units  $\text{XO}_4$  or their derivatives.<sup>10</sup> The NASICON structure contains two distinct positions for monovalent ions usually called Na1 and Na2 sites. In contrast, multivalent ions like magnesium or calcium typically only occupy the Na1-position within the NASICON framework because of their higher charge. This leads to a lower occupation of crystal sites<sup>11</sup> with the Na2 site becoming energetically much more unfavorable for bivalent ions, except for some sulfur structures in which Na2 positions can also be occupied as they are also energetically favorable.<sup>12</sup> The missing occupation of the Na2 sites leads to a higher structural rigidity of the crystal structure which reduces structural changes upon intercalation/de-intercalation. Furthermore, this also leads to a different energetic shape of the diffusion path, as there is no intermediate stable state at Na2, and to a less facile migration caused by the increased electrostatic interactions with the framework.<sup>11</sup>

In times of energy crisis and more demand for electrical storage both in homes and vehicles, the design of new battery systems which do not rely on lithium and, more importantly, on the fast depleting cobalt are in high demand.<sup>7</sup> An obvious choice for higher capacity, especially when the size of the battery is important, are multivalent charge carriers. A promising candidate here is calcium<sup>13,14</sup> as it additionally does not form dendrites and is very abundant in the earth's crust. Furthermore, all-solid batteries have drawn a lot of attention in recent times<sup>15</sup> and the NASICON structure is a popular choice as a solid electrolyte which has been tested intensively with different transition metals, dopants as well as partial or full exchange of charge carriers.<sup>14,16</sup> It can also be utilized as an electrode material under the constraint of electronic conductivity.<sup>12</sup> However, batteries based on multivalent charge carriers are plagued by a lower ion mobility in solid battery materials due to their larger electrostatic interaction with the host lattice.<sup>17,18</sup>

This work explores potential differences in ion mobility within NASICON phases where sodium is fully substituted by calcium. NASICON materials offer a wide range of transition metal options, and we focus on comparing the zirconium-based phase with the titanium-

based phase because of their shared group in the periodic table, meaning they contribute the same number of electrons to redox reactions. However, their different atomic sizes may influence ion mobility, particularly with respect to the so-called bottleneck size. This work aims to investigate how these size differences impact the overall ion mobility within the system.

## Computational details

All phases were studied using periodic density functional theory,<sup>19,20</sup> as implemented in the Vienna *Ab initio* Simulation Package,<sup>21,22</sup> which has been shown to be well-suited to model the properties of batteries.<sup>23</sup> The electron-core interactions are represented by the Projector Augmented Wave (PAW)<sup>24</sup> method. Calculations were first performed for the rhombohedral unit cells of the two NASICON phases consisting of 6 formula units each with the Brillouin zone sampled using a  $4 \times 4 \times 1$  k-point grid. For adsorption, intercalation and ion diffusion, different supercells, which are specified in the respective sections, were used and the k-point grid was scaled accordingly in each lattice direction.

The electronic structure was converged to  $1 \times 10^{-5}$  eV, applying a plane-wave cutoff energy of 550 eV. The migration barriers for intercalation and bulk diffusion were obtained by applying the climbing image Nudged Elastic Band (NEB) method.<sup>25</sup> Most NEB calculations were performed using three distinct images along the pathway. The ones which required more detailed calculations, were found in preliminary setups, to be symmetrical with a meta stable state in the middle and were thus calculated in a symmetrical fashion, from the start point to the meta stable intermediate state. All forces on the atoms were converged within  $0.05 \text{ eV \AA}^{-1}$ .

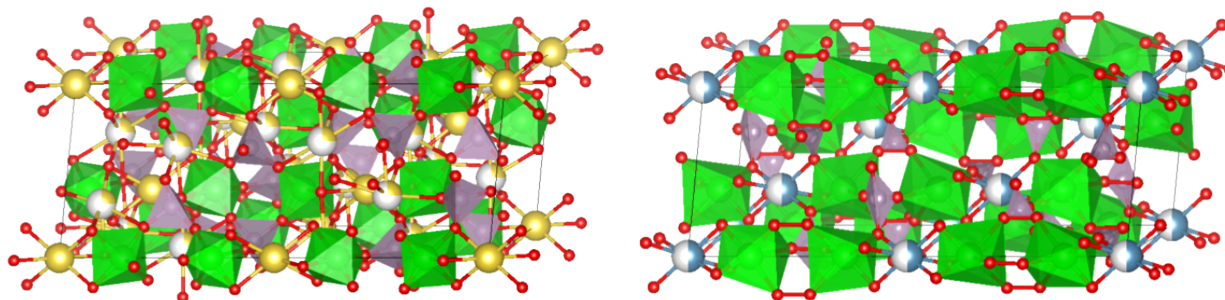


Figure 1: Left: Rhombohedral Unit cell of the classical NASICON Phase. Na1 sites are fully occupied, Na2 sites partially. Right: Rhombohedral unit cell of the NASICON phase with Mg or Ca instead of Na. Na1 sites are half occupied, Na2 sites are not occupied in the ground state.

## Results and Discussion

### Ordering

In this paper, we consider Ca insertion in the classical NASICON structures of  $\text{Ca}_y\text{M}_2(\text{PO}_4)_3$  with  $\text{M} = \text{Ti}$  and  $\text{Zr}$  adapted from experimental XRD data.<sup>26</sup> As already mentioned above, they have been chosen because they have the same number of valence electrons but differ in size with the Zr ion being about 15 % larger than the Ti ion. The considered phases show a rhombohedral structure. As the acronym NASICON, sodium (Na) super ionic conductor, already suggests, these materials have originally been used as solid electrolytes for sodium ion batteries.<sup>27</sup> However, they have recently also become of interest as possible electrode materials for calcium-ion batteries.<sup>12</sup> Given the oxidation states of the considered elements, the Ca-NASICON structures will in general be able to remain electrostatically neutral for an occupation of  $0.5 \leq y \leq 2.5$  calcium per formula unit.

The rhombohedral unit cell of the NASICON structure contains six formula units (see Fig. 1). With the monovalent sodium NASICON structure, at least one Na atom per formula unit is needed to form a charge neutral cell. However, for the divalent Ca and Mg cations only half a cation per formula unit (or one cation per two formula units) is needed. It is still typical to refer the Ca stoichiometry to one formula unit as in  $\text{Ca}_y\text{M}_2(\text{PO}_4)_3$ ,<sup>12</sup> which then results in a nomenclature in which a site occupancy of 0.5 is assumed. This nomenclature

is also motivated by the results of X-ray diffraction (XRD) experiments which yield that the Ca atom can sit at equivalent Na1 sites of the sodium atom in the standard NASICON phase yielding a likelihood of 0.5 for occupation of one particular site.<sup>26</sup> These Na1 sites in a traditional NASICON phase (6B Wyckoff site) sit in an elongated octahedra while the so-called Na2 sites are left empty and only passed during diffusion from one Na1 site to the next in the studied systems.

In our calculations, the previously described rhombohedral NASICON structure ( $R\bar{3}c$ ) ( $\text{Ca}_x\text{M}_{12}(\text{PO}_4)_{18}$ ) containing six NASICON formula units was utilized for all calculations. We also use this stoichiometry to denote the Ca concentrations  $x$  considered in this computational study as it avoids ambiguity associated with the 0.5 occupancies when discussing the differently occupied systems at the high vacancy limit. In the  $y=0.5$  occupancy are three cations to be distributed among six distinct sites, which are all equal in energy for a single occupancy within the rhombohedral unit cell, yielding 20 possible distinct occupation patterns inside the unit cell. However, the variation in the mutual distances between the three cations depending on the particular distribution leads to a variation in the interaction strength causing an energetic ordering of these symmetrically inequivalent occupation patterns. Our calculations showed that the occupation patterns, where alternating sites along the  $z$  axis are occupied are the most stable. This is most likely due to their maximum distance between the cations. They are closely followed in stability by the systems in which two neighboring sites are occupied and the most unstable variations are present when the cations sit right next to each other. However, these stabilities vary by less than 5 meV per atom (see Tab. 1) and suggest that the preference for the cations to be spread equally inside

**Table 1: Differences between the orderings in meV per atom in the  $\text{Ca}_3\text{M}_{12}(\text{PO}_4)_{18}$  unit cells**

	M=Ti	M=Zr
first step	4.1	3.6
second step	2.0	6.5

the unit cell with no clustering is present but small.

In order to verify the most stable configurations, we employed a larger  $2 \times 2 \times 1$  super cell for the NASICON structure. Initially, various occupation scenarios were randomly selected as well as the options with the highest symmetry. Those were cells with alternating layers fully filled as well as neighboring layers fully filled. In total 95 potential occupation arrangements were investigated. Within this context, the cations exhibited a preference for repeatedly occupying the same site within in neighboring unit cells, which led to the formation of distinct layers. Among these configurations, the most stable arrangement involved three layers that were fully occupied while their alternating three layers remained entirely empty. However the total difference between the highest and lowest energy per atom in the system varied by less than 10 meV, indicating the weak mutual interaction between the Ca atoms.

The open-circuit voltage with respect to a Ca metal anode for an occupation from 0 to 6 Ca per rhombohedral unit cell was checked for possible use as an electrode material. The trends are the same for both phases and the exact voltages are shown in table 2: The first intercalation voltage is very high with 16.4V for the Ti phase and 7.9V for the Zr. Note that these high voltages are simply due to the fact that the NASICON material is extremely unstable in the absence of any inserted ion so that the numbers are of no practical relevance. The second and third insertion voltages are both about 4.7 V for both phases. The fourth Ca has a negative voltage and thus is not a stable phase, but it is important to note that for the fourth Ca atom, the Na2 positions become more stable for further occupation than the Na1 positions. Going from the fourth to the fifth Ca the voltage is positive for both phases again, making this transition possible. The occupation with six Ca is most stable with three

**Table 2: Insertion voltages in V for x Ca atoms into the  $\text{Ca}_x\text{M}_{12}(\text{PO}_4)_{18}$  phase with  $\text{M}=\text{Ti},\text{Zr}$**

x	1	2	3	4	5	6
Ti:	16.4	4.7	4.8	-0.9	1.6	1.3
Zr:	7.9	4.6	4.7	-3.0	0.5	0.2

Ca in the Na1 positions and three in the Na2 positions. These voltages show nicely that the material might only be suitable as an electrode in the 1-3 occupation window, but is generally more suitable as a solid electrolyte.

## Diffusion

In a typical NASICON material, the Na cations diffuse through the Na1-Na2-Na1 pathway. In the Ca case, the only difference is that the Na2 equivalent position is much less stable compared to the Na1 position, transforming it into a metastable intermediate state instead of a partially occupied site. Therefore, a full diffusion event takes place between two neighboring Na1 positions. Along the minimum energy path for diffusion, the migrating ion has to pass through a triangular area consisting of the three oxygen atoms in the PO<sub>4</sub> tetrahedron and the TiO<sub>6</sub> or ZrO<sub>6</sub> octahedron, respectively. It has been suggested to consider the area of this bottleneck that corresponds to the structure with the smallest opening along the diffusion pathway as a descriptor for the activation energy for diffusion.<sup>14,28,29</sup> As shown in Figure 2, there are two such bottlenecks in the pathway from Na1 to the Na2 intermediate site. The Na2 octahedron is slightly smaller, so the area of its triangular faces correspond to the defining bottleneck. It is marked as A2 in the figure and has an area of 4.67 Å<sup>2</sup> for the Ti phase and 5.98 Å<sup>2</sup> for the Zr phase. The bottleneck in the Ti phase is thus significantly smaller and only 80% of the area in the Zr phase, suggesting that diffusion will be more hindered in the Ti phase, i.e. associated with a higher diffusion barrier than the Zr phase.

Now we discuss the energy barriers for migration derived by Nudged Elastic Band (NEB) calculations. As a first step we check the diffusion energy of only one cation, to exclude all influence of different occupational environments on the diffusion pathway. This calculation yielded for the Ca<sub>1</sub>Ti<sub>12</sub>(PO<sub>4</sub>)<sub>18</sub> a barrier of 0.92 eV, for Ca<sub>1</sub>Zr<sub>12</sub>(PO<sub>4</sub>)<sub>18</sub> a barrier of 0.71 eV. For both isostructural cells, the energy barriers were roughly the same between all six possible sites with a variance of 5 meV, showing them to be of the same symmetry. Also the prediction of the bottleneck size holds true, as the Zr barrier is only 77 % as high



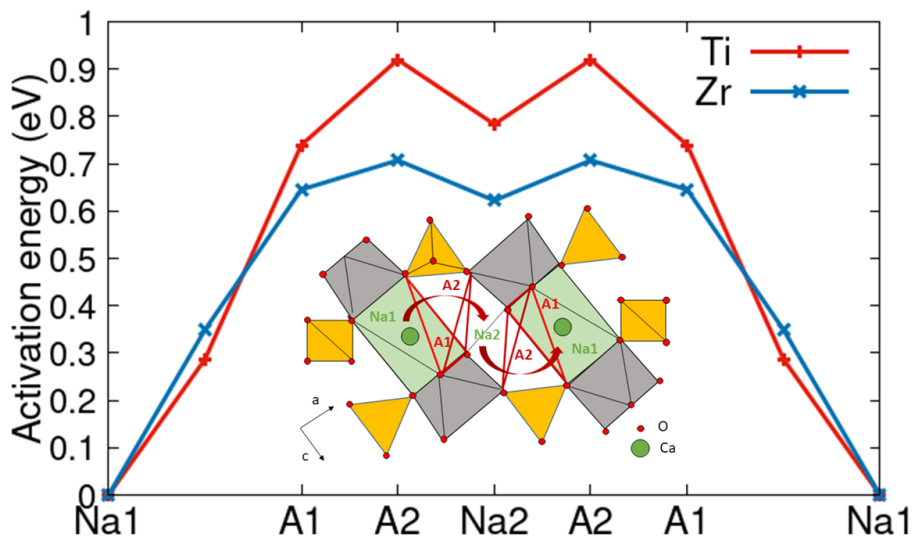


Figure 2: NEB pathway of the diffusion event for one Ca moving through the two bottlenecks and the metastable intermediate in the different phases with a representation of the diffusion pathway of Ca through the NASICON structures. Ca moves through the first octahedra plane A1, then A2 into the unoccupied meta stable Na2 equivalent site, then again through A2 and A1 into the next Na1 equivalent Ca site. The bottleneck of the diffusion is A2, because of its slightly smaller size. The yellow tetraeder and grey octahedra correspond to  $\text{PO}_4$  and the  $\text{TiO}_6$  units or  $\text{ZrO}_6$ , respectively.

as the Ti barrier. Figure 2 shows that the diffusion pathway for one isolated Ca atom is symmetric with respect to the metastable Na2 site. This symmetry can become broken for higher Ca occupations in the simulation cell. For symmetric environments, only half of the total pathway was calculated and then mirrored to the other half to save calculation time. This is the case for most pathways with an occupation of three cations and for all pathways with only one cation present. The following systems with an asymmetrical environment of cations, were determined in two sections with the intermediate positions as an start and end point for ease of calculation.

Adding another cation into the cells creates three distinct pathways of diffusion for each occupational site in the system because of symmetry: The first where the diffusing atom diffuses away from the other cation, the second where it diffuses towards and then the third where the diffusing cation moves parallel to the other cation, which lies in the other half of the unit cell along the z axis and thus has maximum distance to the diffusion pathway.

These three environments are present for all six pathways in the large rhombohedral unit cell. We performed the calculations for the three environments using only one of the six pathways because the calculations with one cation showed those six to be energetically equivalent. As described before, they are asymmetrical pathways where the higher barrier is the determining step. Both isostructural cells (with Ti or Zr) showed the same trend: The closer the additional cation is to the diffusion process, the higher the barrier gets. For the Ti phase the barriers where the cation diffuses towards and away from the additional cation the barriers both lie at 1.01 eV and when the cation is further away on the parallel, the barrier is 0.89 eV. For the Zr phase the farther barriers are 0.76 eV and the closer one is 0.61 eV.

With all three cations present, there are four distinct pathways which can be seen in figure 3. Two of them are symmetric with the two other cations either being on either side of the diffusion process (B), which is very close to the diffusion pathway and in the second case parallel to it (A), which is the furthest the cations can be away from the diffusion. The other two are asymmetric with the cations either directly next to each other (D) or spread out in the phase (C).

In the resulting barrier heights from these possible environments shown in Tab. 3 it can again be confirmed, that in the studied systems the closer the other cations are to the diffusing cation, the higher the barrier is. However with the additional Ca atoms present in the cell further from the diffusion event, the barriers are lower than for the single atom diffusion, showing a stabilizing effect of the environment on the ease of diffusion in the cell. In figure 4 a direct comparison is shown between the minimum diffusion barrier for both

**Table 3: Diffusion barrier in eV for the two isostructural systems  $\text{Ca}_3\text{M}_{12}(\text{PO}_4)_{18}$  for one Ca with two other Ca atoms present in the system**

			M=Ti	M=Zr
symm	far	A	0.64	0.41
	close	B	1.22	0.92
asymm	parallel apart	C	0.98	0.67
	parallel together	D	1.01	0.85

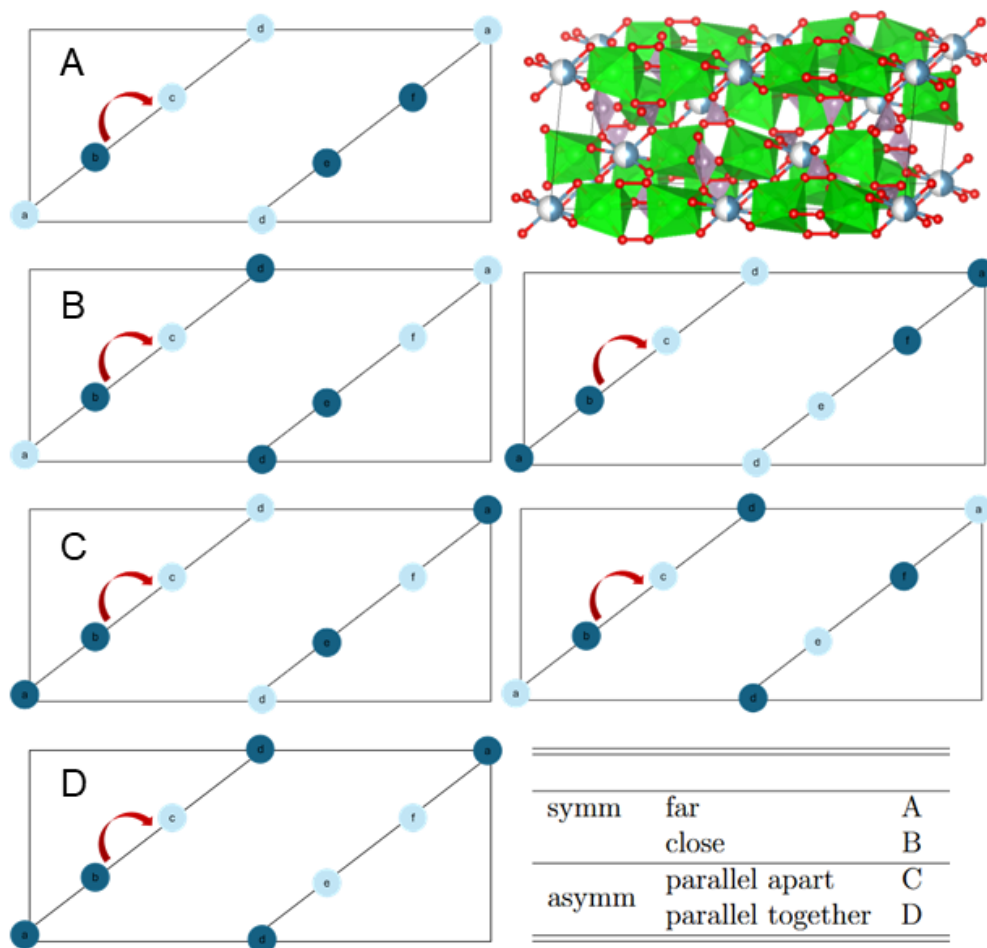


Figure 3: Simplified schematic rhombohedral unit cell showing the four distinct pathway symmetries possible for each diffusion from Na1 to another Na1 site on the example of one specific diffusion event. Bold positions are occupied, faint ones unoccupied. The arrow marks the diffusion.

materials. It can here be seen that the diffusion barrier in the Zr phase are consistently lower than in the Ti phase.

It is also important to note that there is a substantial reduction of the diffusion barriers for higher Ca concentrations. Similar computational results have also been found upon the

**Table 4: Minimum diffusion barrier in eV for the two considered NASICON materials with three different Ca concentrations**

	$x = 1$	$x = 2$	$x = 3$
$\text{Ca}_x\text{Ti}_{12}(\text{PO}_4)_{18}$	0.92	0.89	0.64
$\text{Ca}_x\text{Zr}_{12}(\text{PO}_4)_{18}$	0.71	0.61	0.41

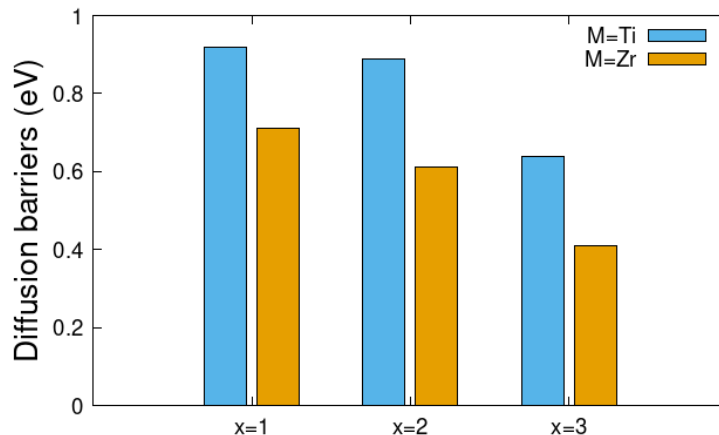


Figure 4: Minimum diffusion barrier in eV for the two considered NASICON materials  $\text{Ca}_x\text{M}_{12}(\text{PO}_4)_{18}$  with three different Ca concentrations  $x=1,2,3$  ( $M=\text{Ti}/\text{Zr}$ )

co-intercalation of Na into  $\text{Ca}_x\text{Na}_y\text{V}_2(\text{PO}_4)_3$  phases<sup>30</sup> and are congruent with the results of the insertion voltages. A study of the NASICON type material as a cathode material for Ca batteries showed similar behavior for  $\text{Ca}_x\text{V}_2(\text{PO}_4)_3$  but the opposite behavior has been observed for  $\text{Ca}_x\text{Mn}_2(\text{PO}_4)_3$ <sup>12</sup>. This is a hint that the studied materials are indeed more suited as a solid electrolyte rather than a electrode material.

## Conclusions and Summary

In this computational study we have addressed the Ca mobility in NASICON battery materials from first principles. Due to the complex structure of the NASICON material, the determination of the Ca migration paths is computationally rather demanding, limiting the number of systems that can be numerically studied. In particular, we considered the Ca mobility in Ti and Zr-based NASICON materials. These two metals have the same number of valence electrons but different sizes, the Zr ion is about 14% larger than the Ti ion which makes the crystal structure more open. According to our calculations, the triangular faces of the so-called Na2 octahedra correspond to the bottleneck along the diffusion path with the area of the faces of the  $\text{TiO}_6$  octahedron being 20% smaller than those of the  $\text{ZrO}_6$  octahedron. In fact, we find that the Zr barrier for Ca diffusion is 23% smaller than the

Ti barrier, confirming the notion that the size of the bottlenecks acts as a good descriptor for the ion mobility. This suggests that increasing the size of the bottlenecks, for example by deliberately doping the NASICON material with larger metal ions, provides a route for increasing the ion mobility in these structures.

## Acknowledgments

This work contributes to the research performed at CELEST (Center for Electrochemical Energy Storage Ulm-Karlsruhe) and was funded by the Deutsche Forschungsgemeinschaft (DFG, German Research Foundation) under Germany's Excellence Strategy – EXC 2154 – Project number 390874152 (POLiS Cluster of Excellence). The computer time was provided by the state of Baden-Württemberg through bwHPC and the German Research Foundation (DFG) through grant no INST 40/575-1 FUGG (JUSTUS 2 cluster).

## Data availability

The data that support the findings of this study will be openly available on NOMAD <https://nomad-lab.eu/nomad-lab/>

## References

- (1) Goodenough, J. B.; Park, K.-S. The Li-Ion Rechargeable Battery: A Perspective. *J. Am. Chem. Soc.* **2013**, *135*, 1167–1176.
- (2) Larcher, D.; Tarascon, J.-M. Towards greener and more sustainable batteries for electrical energy storage. *Nat. Chem.* **2015**, *7*, 19–29.
- (3) Vaalma, C.; Buchholz, D.; Weil, M.; Passerini, S. A cost and resource analysis of sodium-ion batteries. *Nat. Rev. Mat.* **2018**, *3*, 18013.

- (4) Vinayan, B. P.; Euchner, H.; Zhao-Karger, Z.; Cambaz, M. A.; Li, Z.; Diemant, T.; Behm, R. J.; Groß, A.; Fichtner, M. Insights into the electrochemical processes of rechargeable magnesium–sulfur batteries with a new cathode design. *J. Mater. Chem. A* **2019**, *7*, 25490–25502.
- (5) Maroni, F.; Dongmo, S.; Gauckler, C.; Marinaro, M.; Wohlfahrt-Mehrens, M. Through the Maze of Multivalent-Ion Batteries: A Critical Review on the Status of the Research on Cathode Materials for Mg<sup>2+</sup> and Ca<sup>2+</sup> Ions Insertion. *Batteries Supercaps* **2021**, *4*, 1221–1251.
- (6) Ma, Y.; Ma, Y.; Euchner, H.; Liu, X.; Zhang, H.; Qin, B.; Geiger, D.; Biskupek, J.; Carlsson, A.; Kaiser, U. et al. An Alternative Charge-Storage Mechanism for High-Performance Sodium-Ion and Potassium-Ion Anodes. *ACS Energy Lett.* **2021**, *6*, 915–924.
- (7) Esser, B.; Ehrenberg, H.; Fichtner, M.; Groß, A.; Janek, J. Post-Lithium Storage—Shaping the Future. *Adv. Energy Mater.* **2024**, *14*, 2402824.
- (8) Wang, Y.; Song, S.; Xu, C.; Hu, N.; Molenda, J.; Lu, L. Development of solid-state electrolytes for sodium-ion battery – A short review. *Nano Mater. Sci.* **2019**, *1*, 91–100.
- (9) Alamo, J. Chemistry and properties of solids with the [NZP] skeleton. *Solid State Ion.* **1993**, *63*, 547–561.
- (10) Entwistle, J.; Zhang, L.; Zhang, H.; Tapia-Ruiz, N. In *Comprehensive Inorganic Chemistry III (Third Edition)*; Reedijk, J., Poeppelmeier, K. R., Eds.; Elsevier: Oxford, 2023; pp 199–215.
- (11) Sotoudeh, M.; Baumgart, S.; Dillenz, M.; Döhn, J.; Forster-Tonigold, K.; Helmbrecht, K.; Stottmeister, D.; Groß, A. Ion Mobility in Crystalline Battery Materials. *Adv. Energy Mater.* **2024**, *14*, 2302550.

- (12) Tekliye, D. B.; Kumar, A.; Weihang, X.; Mercy, T. D.; Canepa, P.; Sai Gautam, G. Exploration of NaSICON Frameworks as Calcium-Ion Battery Electrodes. *Chem. Mater.* **2022**, *34*, 10133–10143.
- (13) Bier, D.; Li, Z.; Klyatskaya, S.; Sbei, N.; Roy, A.; Riedel, S.; Fichtner, M.; Ruben, M.; Zhao-Karger, Z. Long Cycle-Life Ca Batteries with Poly(anthraquinonylsulfide) Cathodes and Ca-Sn Alloy Anodes. *ChemSusChem* **2023**, *16*, e202300932.
- (14) Wei, Z.; Singh, D. K.; Helmbrecht, K.; Sann, J.; Yusim, Y.; Kieser, J. A.; Glaser, C.; Rohnke, M.; Groß, A.; Janek, J. In Situ Observation of Room-Temperature Magnesium Metal Deposition on a NASICON/IL Hybrid Solid Electrolyte. *Adv. Energy Mater.* **2023**, *13*, 2302525.
- (15) Janek, J.; Zeier, W. A. A solid future for battery development. *Nat. Energy.* **2016**, *1*, 16141.
- (16) Jian, Z.; Hu, Y.-S.; Ji, X.; Chen, W. NASICON-Structured Materials for Energy Storage. *Adv. Mater.* **2017**, *29*, 1601925.
- (17) Bachman, J. C.; Muy, S.; Grimaud, A.; Chang, H.-H.; Pour, N.; Lux, S. F.; Paschos, O.; Maglia, F.; Lupart, S.; Lamp, P. et al. Inorganic Solid-State Electrolytes for Lithium Batteries: Mechanisms and Properties Governing Ion Conduction. *Chem. Rev.* **2016**, *116*, 140–162.
- (18) Sotoudeh, M.; Groß, A. Descriptor and Scaling Relations for Ion Mobility in Crystalline Solids. *JACS Au* **2022**, *2*, 463–471.
- (19) Hohenberg, P.; Kohn, W. Inhomogeneous Electron Gas. *Phys. Rev.* **1964**, *136*, B864–B871.
- (20) Kohn, W.; Sham, L. J. Self-Consistent Equations Including Exchange and Correlation Effects. *Phys. Rev.* **1965**, *140*, A1133–A1138.

- (21) Kresse, G.; Furthmüller, J. Efficient iterative schemes for ab initio total-energy calculations using a plane-wave basis set. *Phys. Rev. B* **1996**, *54*, 11169–11186.
- (22) Kresse, G.; Joubert, D. From ultrasoft pseudopotentials to the projector augmented-wave method. *Phys. Rev. B* **1999**, *59*, 1758–1775.
- (23) Euchner, H.; Groß, A. Atomistic modeling of Li- and post-Li-ion batteries. *Phys. Rev. Mater.* **2022**, *6*, 040302.
- (24) Blöchl, P. E. Projector augmented-wave method. *Phys. Rev. B* **1994**, *50*, 17953–17979.
- (25) Sheppard, D.; Terrell, R.; Henkelman, G. Optimization methods for finding minimum energy paths. *J. Chem. Phys.* **2008**, *128*, 134106.
- (26) Rashmi, C.; Shrivastava, O. Synthesis and crystal structure of nanocrystalline phase:  $\text{Ca}_{1-x}\text{M}_x\text{Zr}_4\text{P}_6\text{O}_{24}$  (M = Sr, Ba and x = 0.0–1.0). *Solid State Sci.* **2011**, *13*, 444–454.
- (27) Singh, B.; Wang, Z.; Park, S.; Gautam, G. S.; Chotard, J.-N.; Croguennec, L.; Carlier, D.; Cheetham, A. K.; Masquelier, C.; Canepa, P. A chemical map of NaSICON electrode materials for sodium-ion batteries. *J. Mater. Chem. A* **2021**, *9*, 281–292.
- (28) Martinez-Juarez, A.; Pecharrromán, C.; Iglesias, J. E.; Rojo, J. M. Relationship between Activation Energy and Bottleneck Size for  $\text{Li}^+$  Ion Conduction in NASICON Materials of Composition  $\text{LiMM}'(\text{PO}_4)_3$ ; M, M' = Ge, Ti, Sn, Hf. *J. Phys. Chem. B* **1998**, *102*, 372–375.
- (29) Wang, Q.; Gao, H.; Li, J.; Liu, G.-B.; Jin, H. Importance of Crystallographic Sites on Sodium-Ion Extraction from NASICON-Structured Cathodes for Sodium-Ion Batteries. *ACS Appl. Mater. Interfaces* **2021**, *13*, 14312–14320.
- (30) Blanc, L. E.; Choi, Y.; Shyamsunder, A.; Key, B.; Lapidus, S. H.; Li, C.; Yin, L.; Li, X.; Gwalani, B.; Xiao, Y. et al. Phase Stability and Kinetics of Topotactic Dual  $\text{Ca}^{2+}$ - $\text{Na}^+$  Ion Electrochemistry in NaSICON  $\text{NaV}_2(\text{PO}_4)_3$ . *Chem. Mater.* **2023**, *35*, 468–481.